

Macro-scale Topology Optimization for Controlling Internal Shear Stress in a Porous Scaffold Bioreactor

K. Youssef², J.J. Mack³, M.L. Iruela-Arispe³, L.-S. Bouchard^{1,2}

Departments of Chemistry and Biochemistry¹, Biomedical Engineering² and Molecular, Cell and Developmental Biology³, University of California, Los Angeles, CA 90095

Shear stress is an important physical factor that regulates proliferation, migration and morphogenesis [1-3]. In regenerative medicine, one approach to generate 3D tissues has been to seed a porous scaffold with cells and growth factors under pulsatile flow conditions [4-6]. However, the resulting bioreactors frequently lack information on intrinsic shear stress and flow distributions. Recent studies have focused on optimizing the microstructural parameters of the scaffold to gain more control over the shear stress [7-9]. In this study, we adopt a different approach whereby macroscopic flows are redirected throughout the bioreactor along patterned channels in the scaffold that result in optimized shear stress distributions. A topology optimization algorithm coupled to effective-medium Lattice Boltzmann simulations was devised to find an optimal channel design that yields a target shear stress that is uniformly distributed throughout the scaffold. The channel topology in the porous scaffold was varied using a combination of genetic algorithm and fuzzy logic. Unlike methods based on varying micro-architectures, the described approach has the ability to achieve a target shear stress and to distribute the shear stress uniformly throughout the scaffold. The ability of topology optimization to alter the shear stress distribution is implemented in experiments where magnetic resonance imaging (MRI) is used to image the flow field.

I. Introduction

Mechanical stimulation of cells has been an important aspect of regenerative medicine and tissue reconstruction [1-3]. Several groups have focused on perfusion bioreactors to employ flow-induced shear stresses on cells residing within a porous matrix [4-6]. The research has clearly demonstrated that shear stress is an important regulator of cell function and a relevant component for pre-conditioning cells prior to implantation in whole animals [10-15].

In previous work, local shear stresses were defined as a function of media flow rate and dynamic viscosity, bioreactor configuration and porous scaffold micro-architecture. The target shear stress values were estimated as averages over the entire scaffold and changes in the overall average were achieved by varying the scaffold micro-architecture under similar flow rates [16]. Recent studies, however, have demonstrated the presence of complex internal microfluidic patterns within the architecture of the porous scaffolds that can clearly alter cell growth in culture [17-18]. Although modeling of scaffold architecture and flow conditions have been considered, no published work to our knowledge has systematically optimized the macro-architecture of channel topology within a porous scaffold to achieve a target shear stress under defined flow inputs.

Here we present a new method to create channel topologies that yields a desired shear stress. The design of optimal channel topology was guided by a genetic algorithm (GA). Shear stress distribution was tested using the Lattice-Boltzmann Method (LBM) to

simulate resulting flow conditions within the scaffold.

The GA achieves the optimization through minimizing a non-conventional cost function based on fuzzy logic rules. The resulting designs show that it is possible to obtain a target shear stress with a much narrower distribution than in the case of a non-optimized topology. The method could potentially be adapted to generate any desired distribution of target internal shear stresses by modification of the cost function. The changes in the shear stress distributions under real flow conditions in porous scaffolds are demonstrated experimentally using magnetic resonance imaging (MRI).

II. Methods

2.1 Lattice Boltzmann Method (LBM)

A computational fluid dynamics (CFD) program was developed based on LBM for flows through porous media [19]. No-slip boundary conditions were implemented. A D2Q9 Bhatnagar-Gross-Krook (BGK) scheme that satisfies the evolution equation of the density distribution function and the conditions shown in equations (1) was adopted, where f_i is the density distribution function, f_i^e is the equilibrium density distribution function, ρ is the density, u is speed, c is velocity direction, and $\omega = 1/t$, where t is the time scale. These conditions lead to a generic family of LBGK equilibria that can be expressed by equation (2), where Q_i is the projector along the i^{th} discrete direction. For the case of a D2Q9, values

for the weights w_i and the speed of sound c_s are fixed according to equations (2).

$$\begin{aligned}\Delta_i f_i &= -\omega(f_i - f_i^e), \\ \sum_i f_i^e &= \sum_i f_i = \rho, \\ \sum_i f_i^e c_{ia} &= \sum_i f_i c_{ia} = \rho u_a \\ f_i^e &= \rho w_i \left(1 + \frac{c_{ia} u_a}{c_s^2} + \frac{Q_{iab} u_a u_b}{2c_s^4}\right),\end{aligned}\quad (1)$$

$$c_s^2 = \frac{1}{3}; w_9 = \frac{4}{9}; w_{1,2,3,4} = \frac{1}{9}; w_{5,6,7,8} = \frac{1}{36}\quad (2)$$

The program was validated by testing it against textbook problems that have known analytical solutions. Shear stress was calculated under the Newtonian fluid assumption using equation (3), where τ is the shear stress tensor, ν is the dynamic viscosity and U is the 2D velocity vector field. The derivatives of the velocity field for the gradient were calculated using finite differences formulae for the four partial derivatives for each fluid point in the lattice as shown in equations (4). Simulations were performed on a 128×128 lattice.

$$\tau = \nu \left(\frac{\nabla U + \nabla U^T}{2} \right)\quad (3)$$

$$\begin{aligned}\frac{\partial U_x(i,j)}{\partial x} &\approx \frac{U_x(i+1,j) - U_x(i-1,j)}{2}, \\ \frac{\partial U_x(i,j)}{\partial y} &\approx \frac{U_x(i,j+1) - U_x(i,j-1)}{2}, \\ \frac{\partial U_y(i,j)}{\partial x} &\approx \frac{U_y(i+1,j) - U_y(i-1,j)}{2}, \\ \frac{\partial U_y(i,j)}{\partial y} &\approx \frac{U_y(i,j+1) - U_y(i,j-1)}{2}\end{aligned}\quad (4)$$

2.2 Generation of the Channel Topology

A method to generate different channel topologies has been developed which works as follows. The method generates a number of individual curves that are superimposed on top of each other, to form a complete topology. Each curve is represented by a vector of length equal to half the length of the lattice. This vector is obtained by calculating the inverse discrete cosine transform (IDCT) of a second vector of the same length. The second vector is filled with zeros, except in a given window near the start of the vector; these entries determine the lower frequency components of the curve. The number of frequency components used

determines the complexity of the curve, which is the maximum number of turns it can make.

A number of curves are first obtained, as shown in Fig. 1. The obtained curves are then superimposed on top of each other, as shown in Fig. 2. The superimposed curves form one fourth of the lattice. They are then symmetrically replicated to cover the complete lattice shown in Fig. 3. Finally, image processing techniques are used to obtain the desired channel width as shown in Fig. 4.

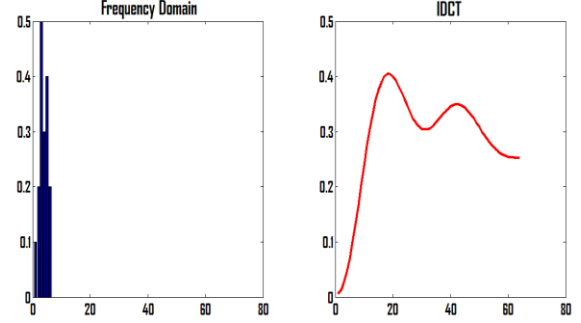


Figure 1. The curve on the right is determined by taking the IDCT of the vector on the left, where only the first six elements (in this particular case) have non-zero values.

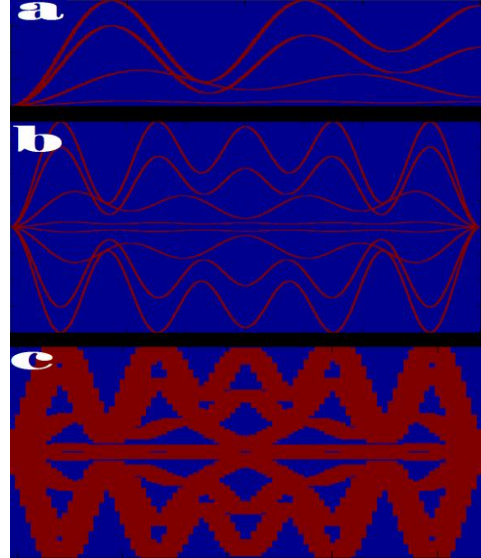


Figure 2. (a) Four curves superimposed on top of each other followed by (b) symmetrical replication to yield (c) the final result.

2.3 Topology Optimization by Genetic Algorithm (GA)

A GA is used to find an optimal channel configuration under a set of predefined requirements and parameters, such as porosity, channel width, number of channels and flow rate. The GA searches in an evolutionary manner for a set of frequency components that generate a channel topology using the mechanism described in section 2.2, to obtain an

optimal channel geometry that yields a uniform target shear stress throughout the scaffold.

The GA starts with a population of random solutions in the search space. It then converges toward a more optimal solution by evaluating the performance of each member in the population and passing the best two members to the next generation in a survival-of-the-fittest manner. The genes of the members with the best performance are crossed over, and a random mutation process with a very low probability is implemented. The resulting offsprings are added to the population as new members. As the number of generations increases, members with better performance evolve. A visual illustration of the evolutionary process carried on by the GA is shown in Figure 3, where the shear stress histograms and distributions for the top members in progressing generations are shown.

Each member in the population represents a channel topology. The performance of each member is evaluated by simulating the flow through a scaffold employing the channel topology it represents, using the LBM. The performance of a shear stress distribution obtained from the simulation is ranked according to a cost function. The goal is to find the channel topology that result in a minimum of the cost function (hopefully, a global minimum). If an appropriate cost function is used, members producing lower costs will have shear stresses that are more uniform, and closer to the target shear stress on average. However, the optimality is directly dependent on the cost function. Thus, using different cost functions can greatly alter the results. The selection of cost function can be a challenging task, depending on the application.

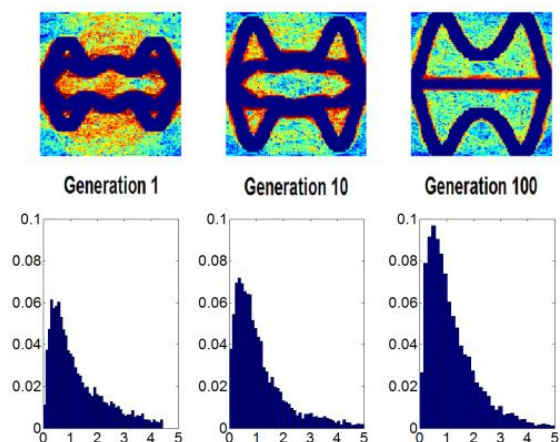


Figure 3. Topology optimization by genetic algorithm: shear stress histograms and distributions after 1, 10, and 100 generations.

2.4 Cost Function

Among popular cost functions is the L-1 norm. The L-1 norm error can be used to measure the

difference between the shear stress distribution of a given channel topology and a target shear stress distribution as shown in equation (5), where each point on the lattice is compared with a target shear stress, and the sum of the absolute values of all the points is the L-1 norm error.

$$error = \sum_{i=1}^{lattice\ height} \sum_{j=1}^{lattice\ width} (|shear\ stress(i, j) - target|). \quad (5)$$

The goal of the optimization is to determine a channel topology that produces a desired average shear stress, which is uniformly distributed throughout the scaffold. Although the L-1 norm works, the problem is that convergence may require a large number of iterations.

To make the goal more explicit to the GA, the cost function can be introduced as a combination of the average and the standard deviation as shown in equation (6). Where *mean* stands for the average shear stress and *stdev* stands for standard deviation. The parameters *w1* and *w2* are weights that determine the influence of each of the two parts of the goal on the total error. The weights are found by trial and error.

$$error = w1 \cdot (mean - target) + w2 \cdot \left(\frac{stdev}{mean}\right) \quad (6)$$

The cost function in equation (6) can be interpreted as a decision process that tries to estimate the performance based on two separate values; the $(mean - goal)$ and the $(stdev/mean)$. For example, let's say we decide that the $(mean - goal)$ is a more important factor in determining the error by assigning it a 60% weight and assigning 40% weight to $(stdev/mean)$. This is a linear relation that can be easily represented by equation (6).

Now suppose we want to introduce some variations to the error such as giving more weight to $(stdev/mean)$ when it's exceptionally low. The relation is no longer linear in this case, and cannot be represented by equation (6). This demonstrates that even if the appropriate weights are found for equation (6) the relation between the two values can only be linear, which is not an accurate resemblance of the nonlinear nature of the relation. This problem is solved by using fuzzy logic to model the decision process.

Fuzzy logic can be defined as a mathematical tool for dealing with uncertainty. It provides a mechanism for representing linguistic constructs such as "small," "medium," "good," and "few" to model the uncertainty associated with vagueness and imprecision [20].

The fuzzy logic system evaluates the performance due to a topology based on a set of rules:

Rule 1	<p><i>IF (mean - target) is small</i> <i>AND $\left(\frac{stdev}{mean}\right)$ is small</i> <i>THEN error is small</i></p>
Rule 2	<p><i>IF (mean - target) is big</i> <i>AND $\left(\frac{stdev}{mean}\right)$ is small</i> <i>THEN error is medium</i></p>
Rule 3	<p><i>IF (mean - target) is small</i> <i>AND $\left(\frac{stdev}{mean}\right)$ is big</i> <i>THEN error is medium</i></p>
Rule 4	<p><i>IF (mean - target) is big</i> <i>AND $\left(\frac{stdev}{mean}\right)$ is big</i> <i>THEN error is large</i></p>

Compared to the L-1 norm, the fuzzy logic method showed an average improvement of 15% in standard deviation, where the average stress matches the target shear stress equally well. A comparison of the relation between the $(mean - goal)$ and the $(stdev/mean)$ using equation (6) versus using fuzzy logic is shown in Figure 4.

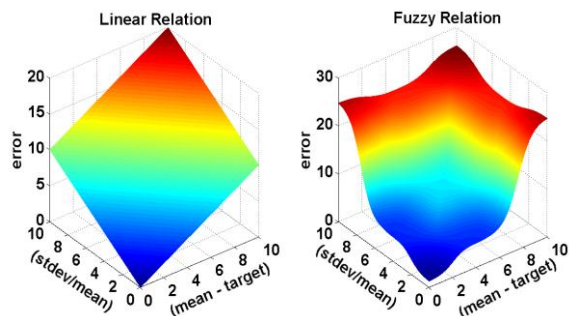


Figure 4. Fuzzy relation vs. linear relation.

2.5 Flow Experiments on Patterned Scaffolds

Our theoretical results were validated using experiments on porous polymer scaffolds, which have been fabricated with flow channels of various topologies. The scaffolds were prepared by a porogen leaching method to achieve high porosity (~90%). Sugar crystals (250-355 μm size distribution) served as the porogen and were added to a 20% wt. solution of polycaprolactone (PCL) in dichloromethane and thoroughly mixed to form a viscous paste (14:1, sugar:PCL). The sugar/PCL paste was then added to a Teflon mold (2cm \times 2cm) embedded with the desired channel topology. A Teflon plunger was applied to uniformly distribute the paste within the mold and compress the sugar

crystals, thereby resulting in an interconnected network of pores after the sugar is removed. Once the paste has been distributed and compressed, the scaffold was allowed to cure via solvent evaporation overnight. To achieve open porosity, the scaffold was leached in deionized water for several days, refreshing the water multiple times a day.

To test the porous scaffolds under flow, a cylindrical bioreactor was custom designed and built. The bioreactor was machined from Teflon in two half-sections to house a 2cm \times 2cm square, 1cm-deep flow chamber, shown in Figure 5. Inlet and outlet ports were drilled through the Teflon to allow the fluid to enter and exit the flow chamber. Plastic tubing was connected via MRI-compatible brass fittings to the inlet and outlet ports. To perform the flow experiments, the scaffold of interest was placed at the base of the flow chamber so that the inlet and outlet were centered at the top scaffold surface. To fill the chamber, two non-channeled porous scaffolds were then added and compressed by tightening four nylon screws to seal the bioreactor.

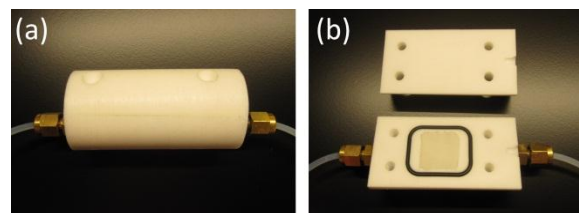


Figure 5. (a) Bioreactor assembled and (b) opened to view porous scaffold within the 2cm \times 2cm flow chamber.

The flow fields inside the scaffolds were mapped by MRI on a Varian 400 MHz (9.4 T) vertical-bore system. A spin echo sequence (MEMS; multi-echo multi-slice) was modified to include flow compensation along all three axes and flow-weighting gradients per user specification. Flow maps were obtained by the method of phase subtraction, in which two images were used, one which is flow-compensated (the reference image), and one in which the gradient first moment (M_1) was set to a value of $M_1=5 \times 10^{-5}$ G \cdot s 2 along x , y and z independently to obtain all three orthogonal components of the flow field as function of space. The flow compensation and flow weighting schemes accounted for the ramp times of each gradient pulse in the MEMS sequence. Only the zeroth and first gradient moments at the center of k -space were matched to the desired values; the higher order moments were ignored.

I. Results

1.1 LBM Simulations

To test the validity of the methods, LBM simulations were performed for three different

configurations. The first configuration is a porous scaffold with no channels. The second configuration is a porous scaffold with manually designed channels: four parallel and straight channels connected to the bioreactor’s inlet and outlet. The third configuration is a porous scaffold with channel topology that was optimized using the methods described herein. The optimization was performed under requirements that will allow comparison with the manually designed channel topology by setting the number of channels and keeping a similar channel width. All configurations were examined with a similar scaffold porosity of 50%. The input velocity was selected for each configuration such that they all share a similar average internal flow velocity that is equal to ~ 1.3 mm/sec. The flow rate diagrams for the three configurations are shown in Figure 7.

The simulation results of the three configurations are shown in Figure 6 (a, b and c). Shear stress histograms are normalized by dividing over the standard deviation to yield a dimensionless quantity. The shear stress maps are shown on a logarithmic scale to simplify the comparison of shear stress values among the three designs. A significant improvement in shear stress uniformity and distribution can be observed in the logarithmic scale graphs for the optimized configuration when compared to the no-channel and manual channel configurations, where a target shear stress value of 2 on the logarithmic scale was set for the optimization.

Improvement can also be seen quantitatively. Figure 6 shows the standard deviation divided by mean shear stress for each configuration. This parameter was calculated as a measurement of distribution uniformity. The parameter value for the case of no channels is 27% larger than the optimized configuration. For the case of the manual design, the parameter value is 46% larger than the optimized configuration.

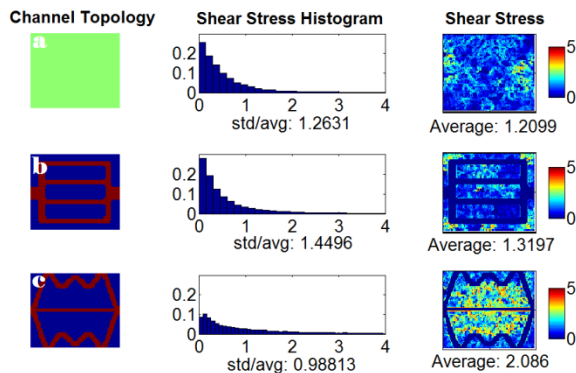


Figure 6. Simulation results for control and optimized topologies, and their corresponding input velocities. (a) No channels (2.59 m/sec); (b) Manual channel design (0.25 m/sec); (c) Optimized channel design (0.62 m/sec).

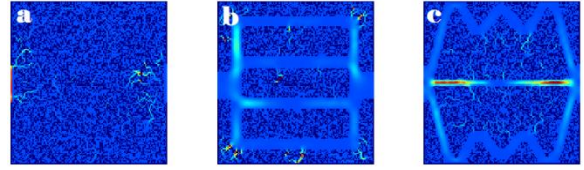


Figure 7. Corresponding flow rate diagrams of the three configurations.

We have observed in all cases that these simulations produce a nonlinear relationship between input pressure and average shear stress. For example, in the case of the no-channel configuration, a point was reached after which increasing input pressure did not produce further increases in the average shear stress through the scaffold. Changing the macro structure of the scaffold by introducing channels can alter the average shear stress limit. By using our optimization method, we were able to systematically increase the average shear stress limit to a desired target average shear stress (whereas without topology optimization, this value remains below the plateau).

Furthermore, the proposed optimization method offers flexibility in the following sense. It can be tuned to control the different aspects of shear stress distribution by modifying the rules of the fuzzy cost function. In other simulations for which the details are not shown in this paper, the cost function was modified to give more weight to minimizing standard deviation. This produced a channel design that yields a std/avg value of ~ 0.7 . We expect to be able to reduce this value even further by increasing the number of channels and reducing the width of the channels. However, this requires an increase in the lattice resolution, which leads to an increase in computation time.

1.2 Flow Rate Simulations

Varying the flow rate at the inlet amounts to varying the applied pressure difference across the bioreactor. The effect of flow rate on channel topology was studied as follows: simulations were performed for 10 different flow rate values that varied from very low to very high were performed. Five simulations for each flow rate value were performed, for a total of 50 simulations. All simulations had the same target shear stress. Uniformity was measured as the ratio between standard deviation and average shear stress. The plot

in Figure 8 shows the relationship between shear stress uniformity and flow rate. Using this plot, the ideal flow rate for a target shear stress value can be determined. The degree of steady performance with the least fluctuations between runs can be identified.

High fluctuations are observed for very low and very high flow rates. The fluctuations at very low flow rates are believed to be due to the fact that diffusion takes over at these rates, where the effect of channel topology diminishes. For very high rates, the fluctuations are likely due to an inability to find a channel topology that can match such high flow rates with the given target shear stress. In other words, if the flow rate is too high for the target shear stress, no channel topology can match them. Instead, the GA will try to get as close as possible, which causes increasingly different results (randomness) from run to run.

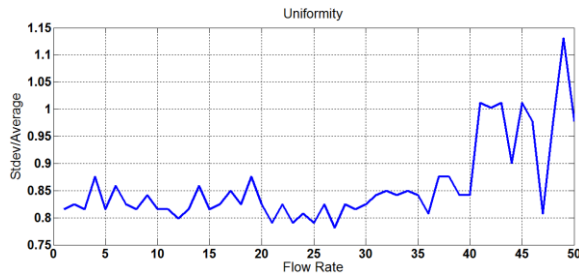


Figure 8. Uniformity variation with increasing flow rates corresponding to ten input velocity values: (0.1, 0.2, 0.3, 0.4, 0.5, 1, 2, 3, 4 and 5) m/s. Value increases every 5 steps.

1.3 Flow Rate Optimization

Next we investigated how the proposed optimization methods can be used to analyze the effect of flow rate on the uniformity of shear stress distribution when the flow rate was no longer fixed. The responsibility of determining the flow rate value is assigned to the GA. In this case, the GA searches for a combination of topology and flow rate that can achieve an optimal distribution for a desired shear stress. The resulting optimal topology is shown in Figure 9, where the suggested flow rate corresponds to an input velocity value of 1.56 m/s.

Improvement could be observed both visually and in the (*stdev/mean*) parameter value. This suggests that removing the constraint of a fixed flow rate gives the GA more freedom in optimizing the design.

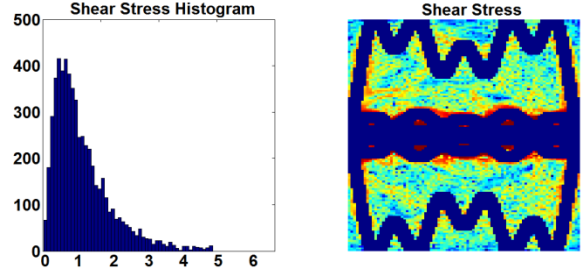


Figure 9: Shear stress histogram and distribution for the optimal topology.

1.5 Flow Imaging Experiments in Fabricated Scaffolds

Each 2cm × 2cm porous scaffold was placed into the bioreactor flow chamber and water was flowed at a constant rate of ~250 mL/min during the image acquisition. The flow chamber was padded using additional non-channeled porous scaffold material to minimize the possibility of water flowing outside the channel region. The channels of the scaffold of interest were aligned with the inlet and outlet of the flow chamber in the bioreactor.

The velocity-field MRI data (2 mm-thick two-dimensional slices, FOV = 25mm × 25mm, 128×64) were imported into MATLAB (The Mathworks, Natick, MA) and used to compute by finite-differences the shear rate in the plane of the slice (aligned with the flow direction) using the formula $\partial_x v_y + \partial_y v_x$. From these MRI-derived maps, the shear rate values in regions outside the flow channels were extracted and histograms were plotted normalized to the number of values. The results are shown in Figure 10.

In the Figure 10 caption we list the values of *std/avg*. It can be seen that the improvement from the manually-designed over the case of no channels is insignificant. On the other hand, a narrower distribution of shear rates is measured in the topology-optimized scaffold [Figure 10(c)]. This demonstrates our ability to control the variance of the shear rate distribution.

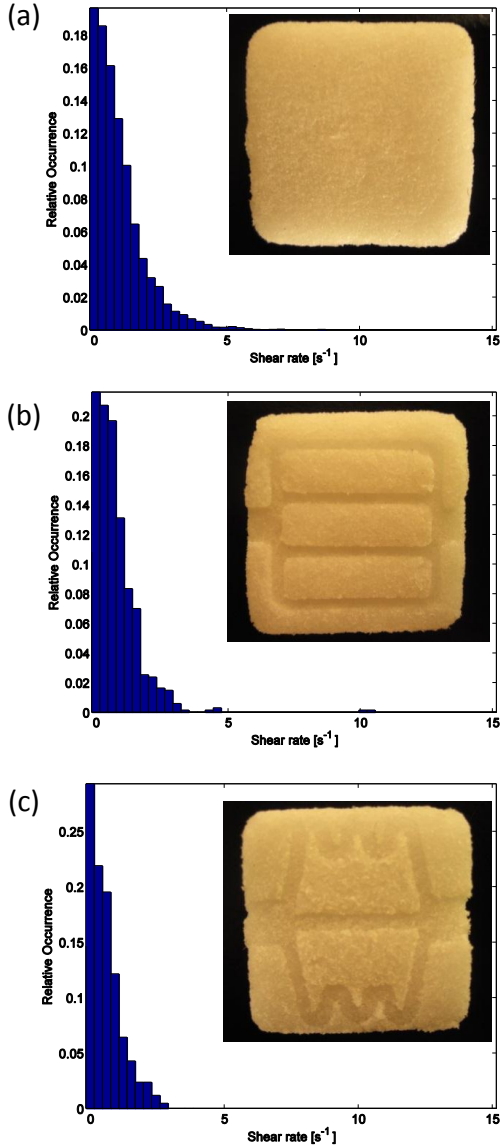


Figure 10. Comparison of MRI-derived shear rate distributions for water flowing in three different porous scaffolds: (a) no channels ($std/avg \sim 0.90$), (b) manual design of the channel topology ($std/avg \sim 0.97$) and (c) topology-optimized channel design ($std/avg \sim 0.80$). In (a-c), a photograph of the $2\text{cm} \times 2\text{cm}$ porous scaffold is inlaid to show the channel topology. The flow rate in each scaffold was 250 mL/min at the inlet, and results in flow velocities in the range $0\text{-}5\text{ mm/s}$ inside the porous scaffold.

I. Discussion

All the simulations in this work are done in two dimensions (2D). The same method could be extended to control shear stress distributions in three dimensions (3D). The primary issue that must be considered when performing computational fluid dynamics in 3D is computation time. LBM offers a big speed advantage over other methods, yet

optimization algorithms need to run thousands of simulations in order to reach an optimal solution. In our case, the population size used in the GA is 20 members, and the number of generations is 100. This gives a total of 2,000 runs. Using a state of the art computer, for a 128×128 lattice, each run takes an average of 9 seconds. This yields a total time of 5 hours to perform one optimization.

Considering the size of the search space, the number of runs performed by the GA is quite low. For example, the number of parameters used by the GA in the flow rate simulations is 28. If we consider a resolution of 10^{-3} for each parameter, this produces a search space of $1,000^{28}$ possibilities. To perform simulations with such computational complexity in 3D, other means of computation must be considered. Particularly, parallel processing is the means of performing such computations. For extending our methods to 3D, one possibility is to use a 400 core GPU. An estimated factor of 50 is expected for speed increase. This means that running a $128 \times 128 \times 128$ 3D lattice requires roughly twice the time currently required by a 128×128 2D lattice. However, it is also expected that for a more complex lattice longer convergence times will be required. Thus, the actual rough expected time for 3D simulations could be up to 20 times the convergence times required for 2D simulations.

In future work, the biological response to the scaffold topology design will be experimentally studied. Control over flow and shear stress within a scaffold is essential in order to correlate cell response to a defined shear stress distribution. By controlling the scaffold macro-architecture, we can control flow in three dimensions and study the effects of shear stress, uniform or varied, on cell growth (i.e. cell proliferation and migration). The ability to vary the scaffold topology allows us to control patterns of shear stress within the scaffold. It is still unknown as to the (spatio-temporal) patterns of shear stress that will facilitate cell growth and proliferation over time, and therefore the ability to alter the flow pattern in both space and time will be paramount to understanding a biological response to flow and correlated mechanical forces. This need for adaptable flow patterns is especially relevant considering cell growth within a scaffold is expected to increase the resistance to flow. To control flow in 3D, multiple inlets can be arranged such that patterns of shear stress are applied to stimulate cell growth within the scaffold and ultimately improve *in vitro* tissue culture.

II. Conclusion

In this paper we present algorithms to provide controlled shear stress distribution in porous

scaffolds through optimization of macro-scale channel topology. Experimental results confirm the validity of our methods in 2D, future work will focus on extending these methods to control shear stress distribution in 3D. Parallel processing techniques are being considered to reduce computation time and extend the optimization method to 3D geometries.

Providing a means to control shear stress through macro-architecture of a scaffold facilitates studying the effect of shear stress distribution on cell proliferation and gene expression under flow in a 3D scaffold. The main advantage of redirecting macroscopic flows is the ability to optimize the shear stresses throughout the entire bioreactor volume without the need to optimize the microstructure while keeping the implementation in the laboratory feasible.

REFERENCES

- [1] M.U. Nollert, S.L. Diamond, L.V. McIntire, "Hydrodynamic Shear Stress and Mass Transport Modulation of Endothelial Cell Metabolism." *Biotechnology and Bioengineering* **38**, 588-602 (1991).
- [2] N. Datta, Q.P. Pham, U. Sharma, V.I. Sikavitsas, J.A. Jansen, A.G. Mikos, "In Vitro Generated Extracellular Matrix and Fluid Shear Stress Synergistically Enhance 3D Osteoblastic Differentiation." *PNAS* **103**, 2488-2493 (2006).
- [3] S. Stolberg, K.E. McCloskey, "Can Shear Stress Direct Stem Cell Fate?" *Biotechnology Progress* **25**, 10-19 (2009).
- [4] G.N. Bancroft, V.I. Sikavitsas, A.G. Mikos, "Design of a Flow Perfusion Bioreactor System for Bone Tissue-Engineering Applications." *Tissue Engineering* **9**, 549-554 (2003).
- [5] S. Dermenioudis, Y.F. Missirlis, "Bioreactors in Tissue Engineering." *Advanced Materials* **12**, B592-B608 (2010).
- [6] M.A. Brown, R.K. Iyer, M. Radisic, "Pulsatile Perfusion Bioreactor for Cardiac Tissue Engineering." *Biotechnology Progress* **24**, 907-920 (2008).
- [7] R.S. Voronov, S.B. VanGordon, V.I. Sikavitsas, D.V. Papavassiliou, "Distribution of flow-induced stresses in highly porous media." *Applied Physics Letters* **97**, 024101 (2010).
- [8] R.S. Voronova, S.B. VanGordona, V.I. Sikavitsasa, D.V. Papavassiliou, "Computational modeling of flow-induced shear stresses within 3D salt-leached porous scaffolds imaged via micro-CT." *Journal of Biomechanics* **43**, 1279-1286 (2010).
- [9] S.B. VanGordon, R.S. Voronov, T.B. Blue, R.L. Shambaugh, D.V. Papavassiliou, V.I. Sikavitsas, "Effects of Scaffold Architecture on Preosteoblastic Cultures under Continuous Fluid Shear." *Ind. Eng. Chem. Res.* **50**, 620-629 (2011).
- [10] K.M. Reich, J.A. Frangos, "Effect of Flow on Prostaglandin E2 and Inositol Trisphosphate Levels in Osteoblasts." *American Journal of Physiology* **261**, C428-C432 (1991).
- [11] M.V. Hillsley, J.A. Frangos, "Alkaline Phosphatase in Osteoblasts is Down-Regulated by Pulsatile Fluid Flow." *Calcified Tissue International* **60**, 48-53 (1997).
- [12] R. Smalt, F.T. Mitchell, R.L. Howard, T.J. Chambers, T.J., "Induction of NO and Prostaglandin E2 in Osteoblasts by Wall-Shear Stress but not Mechanical Strain." *American Journal of Physiology* **273**, E751-E758 (1997).
- [13] J. Klein-Nulend, M.H. Helfrich, J.G. Sterck, H. MacPherson, M. Joldersma, S.H. Ralston, C.M. Semeins, E.H. Burger, "Nitric Oxide Response to Shear Stress by Human Bone Cell Cultures is Endothelial Nitric Oxide Synthase Dependent." *Biochemical and Biophysical Research Communications* **250**, 108-114 (1998).
- [14] T.N. McAllister, T. Du, J.A. Frangos, "Fluid Shear Stress Stimulates Prostaglandin and Nitric Oxide Release in Bone Marrow Derived Preosteoclast-like Cells." *Biochemical and Biophysical Research Communications* **270**, 643-648 (2000).
- [15] G.L. Jiang, C.R. White, H.Y. Stevens, J.A. Frangos, J.A., "Temporal Gradients in Shear Stimulate Osteoblastic Proliferation via ERK 1/2 and Retinoblastoma Protein." *American Journal of Physiology, Endocrinology and Metabolism* **283**, E383-E389 (2002).
- [16] B. Porter, R. Zauel, H. Stockman, R. Guldberg, D. Fyhrie, "3-D Computational Modeling of Media Flow through Scaffolds in a Perfusion Bioreactor." *Journal of Biomechanics* **38**, 543-549 (2005).
- [17] A.F.M.B. Khoda, I.T. Ozbolat, B. Koc, B., "Engineered Tissue Scaffolds with Variational Porous Architecture." *Journal of Biomechanical Engineering* **133**, 011001 (2011).
- [18] F. Okkels, M. Dufva, H. Bruus, H., "Optimal Homogenization of Perfusion Flows in Microfluidic Bio-Reactors: A Numerical Study." *PLoS ONE* **6**, e14574-e14574 (2011).
- [19] S. Succi: *The Lattice Boltzmann Equation for Fluid Dynamics and Beyond. Numerical Mathematics and Scientific Computation.* Oxford University Press, New York, 2001.
- [20] S. N. Sivanandam, S. Sumathi, S. N. Deepa: *Introduction to Fuzzy Logic using MATLAB.* Springer-Verlag, Berlin Heidelberg, 2007.